Electronic Supplementary Material (ESI) for Journal of Materials Chemistry C.

Modeling the tunable thermal conductivity of intercalated layered materials with three-directional anisotropic phonon dispersion and relaxation times

Chengjie Wang[a,c], Maogang He[a], Xiangyang Liu[a], Jonathan A. Malen[b,c,*]

*Corresponding author E–mail: jonmalen@andrew.cmu.edu

[a]MOE Key Laboratory of Thermo-Fluid Science and Engineering, Xi'an Jiaotong University, Xi'an, Shaanxi 710049, PR China, [b]Department of Materials Science and Engineering, Carnegie Mellon University, Pittsburgh, PA, USA 15213, [c]Department of Mechanical Engineering, Carnegie Mellon University, Pittsburgh, PA, USA 15213.

Supplementary information

A. Derivation for the TDA model

The general form of $G_s(\omega)$ (v^2DOS) is a surface integral which can be calculated by projecting the 3D isoenergy surface to a 2D plane (Ref [17]). Here we choose q_a-q_b plane for the projection and take a direction for example, then the surface integral elements can be written as

$$dS_\omega = \sqrt{1+\left(\frac{\partial q_c}{\partial q_a}\right)^2+\left(\frac{\partial q_c}{\partial q_b}\right)^2}\, dq_a q_b \tag{S1}$$

where q_c can be expressed in terms of q_a and q_b, $q_c = \sqrt{\omega^2-\left(v_a^2 q_a^2+v_b^2 q_b^2\right)}/v_c$ and $G_a(\omega)$ is expressed as

$$G_a(\omega)=\frac{1}{8\pi^3}\iint_{S_\omega}\frac{dS_\omega}{\left\|\mathbf{v}_g\right\|}\mathbf{v}_{g,a}^2=\frac{1}{8\pi^3}\iint_{S_\omega}\sqrt{1+\left(\frac{\partial q_c}{\partial q_a}\right)^2+\left(\frac{\partial q_c}{\partial q_b}\right)^2}\,\frac{dq_a q_b}{\left\|\mathbf{v}_g\right\|}\mathbf{v}_{g,a}^2 \tag{S2}$$

The group velocity along the a-axis is $d\omega/dq_a$

$$v_{g,a}=v_a^2 q_a/\omega \tag{S3}$$

The group velocity along the other two directions is similar, so the total group velocity is

$$v_g = \sqrt{v_a^4 q_a^2 + v_b^4 q_b^2 + v_c^4 q_c^2} / \omega \tag{S4}$$

Eq. S2 can be evaluated by implementing the ellipse parametric equations

$$q_a = \frac{1}{v_a} \rho \cos\varphi, q_b = \frac{1}{v_b} \rho \sin\varphi \tag{S5}$$

where ρ is the polar radius and φ is the polar angle. Substituting Eqs. S3-S5 to the Eq. S2, we get

$$G_a(\omega) = \frac{1}{8\pi^3} \int_0^{2\pi} \int_{\rho_{\min}}^{\rho_{\max}} \frac{v_a}{v_b v_c \omega} \sqrt{\frac{1}{\omega^2 - \rho^2}} \rho^3 (\cos\varphi)^2 \, d\rho d\varphi \tag{S6}$$

where the domain of ρ depends on the magnitudes of the isoenergy surface and boundary of the effective FBZ. If cutoff frequencies along the *a, b* and *c*-axis satisfy $\omega_a > \omega_b > \omega_c$, we show three cases to determine the domain of the ρ as shown in Figure S1.

When $\omega < \omega_c$, the whole isoenergy surface is within the effective FBZ, see case 1 in Figure S1, so there is $0 \le \rho \le \omega$. For case 2, when $\omega_c < \omega < \omega_b$, the isoenergy surface exceeds the boundary of the effective FBZ in the *c* direction, and the projection of the isoenergy surface within the effective FBZ to q_a-q_b plane is an annulus whose outer edge is exactly the isoenergy surface projection. The inner edge is the intersecting line of isoenergy surface and the effective FBZ, here we assume it as an ellipse with the same eccentricity as the outer ellipse to simplify the calculation. By solving the intersection of the isoenergy surface and the effective FBZ, the domain of ρ can be determined as $\omega_b \sqrt{(\omega^2 - \omega_c^2)/(\omega_b^2 - \omega_c^2)} \le \rho \le \omega$. As for the case 3: $\omega_b < \omega < \omega_a$, the isoenergy surface lies outside of the effective FBZ along the *b* and *c* directions. We project the isoenergy surface to the q_b-q_c plane, and similarly derive $G_a(\omega)$ as

$$G_a(\omega) = \frac{1}{8\pi^3} \int_0^{2\pi} \int_{\rho_{r,\min}}^{\rho_{r,\max}} \frac{v_a}{v_b v_c \omega} \sqrt{\omega^2 - \rho_r^2} \, \rho_r d\rho_r d\varphi_r \tag{S7}$$

where ρ_r and φ_r are the parameters in ellipse parametric equation similar to ρ and φ in Eq. S5. Using the eccentricity approximation for simplification like case 2, the domain of ρ_r is $0 \le \rho_r \le \omega_{D,b} \sqrt{(\omega^2 - \omega_{D,a}^2)/(\omega_{D,b}^2 - \omega_{D,a}^2)}$.

Based on the determined domain of ρ and ρ_r above, expression for $G_a(\omega)$, $G_b(\omega)$ and $G_c(\omega)$ can be obtained as shown in the main article. Substituting these expressions into Eq. 4, the thermal conductivity along a, b and c direction is

$$k_a = \sum_p \frac{v_a}{6\pi^2 v_b v_c} \frac{k_B^4 T}{\hbar^3} \left[\begin{array}{l} \int_0^{X_c} \frac{T^2 X^4 e^X \tau}{\left(e^X - 1\right)^2} dX + \frac{3T\theta_{D,c}}{2} \int_{X_c}^{X_b} \frac{X^3 e^X \tau}{\left(e^X - 1\right)^2} \left(\frac{\theta_{D,b}^2 - (TX)^2}{\theta_{D,b}^2 - \theta_{D,c}^2} \right)^{\frac{1}{2}} dX \\ - \frac{\theta_{D,c}^3}{2T} \int_{X_c}^{X_b} \frac{X e^X \tau}{\left(e^X - 1\right)^2} \left(\frac{\theta_{D,b}^2 - (TX)^2}{\theta_{D,b}^2 - \theta_{D,c}^2} \right)^{\frac{3}{2}} dX + \int_{X_b}^{X_a} \frac{T^2 X^4 e^X \tau}{\left(e^X - 1\right)^2} dX \\ - \frac{\theta_{D,a}^3}{T} \int_{X_b}^{X_a} \frac{X e^X \tau}{\left(e^X - 1\right)^2} \left(\frac{\theta_{D,b}^2 - (TX)^2}{\theta_{D,b}^2 - \theta_{D,a}^2} \right)^{\frac{3}{2}} dX \end{array} \right] \tag{S8}$$

$$k_b = \sum_p \frac{v_b}{6\pi^2 v_a v_c} \frac{k_B^4 T}{\hbar^3} \left[\begin{array}{l} \int_0^{X_c} \frac{T^2 X^4 e^X \tau}{\left(e^X - 1\right)^2} dX + \frac{3T\theta_{D,c}}{2} \int_{X_c}^{X_b} \frac{X^3 e^X \tau}{\left(e^X - 1\right)^2} \left(\frac{\theta_{D,b}^2 - (TX)^2}{\theta_{D,b}^2 - \theta_{D,c}^2} \right)^{\frac{1}{2}} dX \\ - \frac{\theta_{D,c}^3}{2T} \int_{X_c}^{X_b} \frac{X e^X \tau}{\left(e^X - 1\right)^2} \left(\frac{\theta_{D,b}^2 - (TX)^2}{\theta_{D,b}^2 - \theta_{D,c}^2} \right)^{\frac{3}{2}} dX + \int_{X_b}^{X_a} \frac{T^2 X^4 e^X \tau}{\left(e^X - 1\right)^2} dX \\ - \frac{3T\theta_{D,a}}{2} \int_{X_b}^{X_a} \frac{X^3 e^X \tau}{\left(e^X - 1\right)^2} \left(\frac{\theta_{D,b}^2 - (TX)^2}{\theta_{D,b}^2 - \theta_{D,a}^2} \right)^{\frac{1}{2}} dX \\ + \frac{\theta_{D,a}^3}{2T} \int_{X_b}^{X_a} \frac{X e^X \tau}{\left(e^X - 1\right)^2} \left(\frac{\theta_{D,b}^2 - (TX)^2}{\theta_{D,b}^2 - \theta_{D,a}^2} \right)^{\frac{3}{2}} dX \end{array} \right] \tag{S9}$$

$$k_c = \sum_p \frac{v_c}{6\pi^2 v_a v_b} \frac{k_B^4 T}{\hbar^3} \left[\begin{array}{l} \int_0^{X_c} \frac{T^2 X^4 e^X \tau}{\left(e^X - 1\right)^2} dX + \frac{\theta_{D,c}^3}{T} \int_{X_c}^{X_b} \frac{X e^X \tau}{\left(e^X - 1\right)^2} \left(\frac{\theta_{D,b}^2 - (TX)^2}{\theta_{D,b}^2 - \theta_{D,c}^2} \right)^{\frac{3}{2}} dX \\ + \int_{X_b}^{X_a} \frac{T^2 X^4 e^X \tau}{\left(e^X - 1\right)^2} dX - \frac{3T\theta_{D,a}}{2} \int_{X_b}^{X_a} \frac{X^3 e^X \tau}{\left(e^X - 1\right)^2} \left(\frac{\theta_{D,b}^2 - (TX)^2}{\theta_{D,b}^2 - \theta_{D,a}^2} \right)^{\frac{1}{2}} dX \\ + \frac{\theta_{D,a}^3}{2T} \int_{X_b}^{X_a} \frac{X e^X \tau}{\left(e^X - 1\right)^2} \left(\frac{\theta_{D,b}^2 - (TX)^2}{\theta_{D,b}^2 - \theta_{D,a}^2} \right)^{\frac{3}{2}} dX \end{array} \right] \tag{S10}$$

where X_a is ω_a/T, and X_b and X_c are similar.

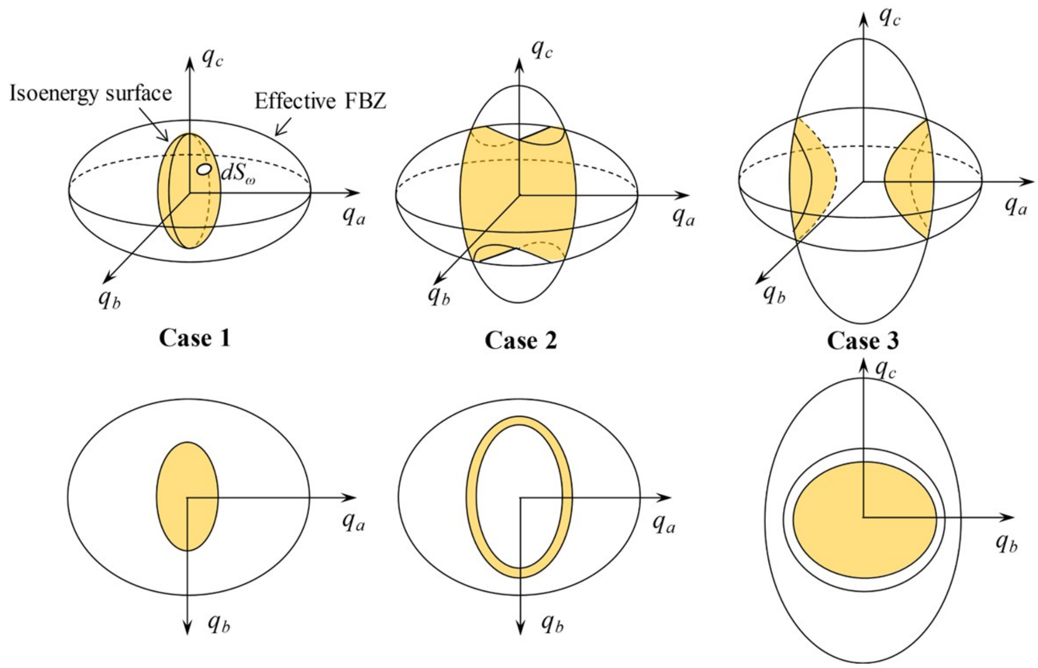

Figure S1. The relationship between the isoenergy surface and the effective FBZ for three frequency regimes. Case 1, all of the states on the isoenergy surface are allowed, the projection to the q_a-q_b plane is an ellipse; Case 2, orange shading on the isoenergy surface is the allowed states, the projection to the q_a-q_b plane is an elliptical ring; Case 3, orange shading on the isoenergy surface is the allowed states, the projection to the q_b-q_c plane is an ellipse.

B. $G_s(\omega)$ using **polynomial and sine function dispersions**

S_ω, the isoenergy surface, can also be defined for a dispersion relationship with arbitrary functional form as $\omega^2 = f_a^2(q_a) + f_b^2(q_b) + f_c^2(q_c)$. We consider two examples here: a polynomial function of the form $f_a(q_a) = A_1 q_a{}^2 + B_1 q_a$ and a sine function of the form $f_a(q_a) = \mathrm{a}_1 \sin(b_1 q_a)$ with b and c directions are similarly defined. For the polynomial dispersion we have,

$$\frac{\left(A_1 q_a{}^2 + B_1 q_a\right)^2}{\omega^2} + \frac{\left(A_2 q_b{}^2 + B_2 q_c\right)^2}{\omega^2} + \frac{\left(A_3 q_c{}^2 + B_3 q_c\right)^2}{\omega^2} = 1 \qquad \text{(S11)}$$

For the sine function dispersion, we have,

$$\frac{\left(\mathrm{a}_1 \sin(b_1 q_a)\right)^2}{\omega^2} + \frac{\left(\mathrm{a}_2 \sin(b_2 q_b)\right)^2}{\omega^2} + \frac{\left(\mathrm{a}_3 \sin(b_3 q_c)\right)^2}{\omega^2} = 1 \qquad \text{(S12)}$$

These assumptions create isoenergy surfaces that are irregular.

Choosing q_a-q_b plane for the projection, so the surface integral elements can also be written as $dS_\omega = \sqrt{1+\left(\frac{\partial q_c}{\partial q_a}\right)^2+\left(\frac{\partial q_c}{\partial q_b}\right)^2}\, dq_a q_b$, and $G_a(\omega)$ can also be expressed as

$$G_a(\omega)=\frac{1}{8\pi^3}\iint_{S_\omega}\sqrt{1+\left(\frac{\partial q_c}{\partial q_a}\right)^2+\left(\frac{\partial q_c}{\partial q_b}\right)^2}\,\frac{dq_a q_b}{\left\|\mathbf{v}_g\right\|}\mathbf{v}_{g,a}^2 \qquad \text{(S13)}$$

The group velocity along the a-axis is $d\omega/dq_a$

$$v_{g,a} = f_a(q_a)\frac{df_a(q_a)}{\omega dq_a} \qquad \text{(S14)}$$

The group velocity along the other two directions is similar, so the total group velocity is

$$v_g=\sqrt{\left[f_a(q_a)\frac{df_a(q_a)}{dq_a}\right]^2+\left[f_b(q_b)\frac{df_b(q_b)}{dq_b}\right]^2+\left[f_c(q_c)\frac{df_c(q_c)}{dq_c}\right]^2}\,/\,\omega \qquad \text{(S15)}$$

By substituting Eqs. S11-S12 and S14-S15 to the Eq. S13, we can determine G_a and similarly G_b and G_c for a dispersion relationship with a specified functional form in the a, b, and c directions. While analytical solutions, similar to those found for linear dispersion may be difficult, numerical evaluation is possible with this framework.

C. Stepwise integration approach to get the accumulation function

Here we restrict the in-plane dispersion to be isotropic to simplify the derivation. Similar to the derivation for $G_a(\omega)$ above, the expression for $G_{ab}(\omega)$ is

$$G_{ab}(\omega)=\frac{1}{8\pi^3}\int_0^{2\pi}\int_0^{q_{ab,\max}}\sqrt{\frac{\omega^2}{v_c^{\,2}\left(\omega^2-v_{ab}^{\,2}q_{ab}^{\,2}\right)}}\,q_{ab}\,dq_{ab}\,d\varphi \qquad \text{(S16)}$$

So the thermal conductivity along the ab direction is

$$k_{ab}=\sum_p\frac{1}{4\pi^2}\int_\omega \hbar\omega\frac{\partial f_{BE}}{\partial T}\tau\int_0^{q_{ab,\max}}\sqrt{\frac{\omega^2}{v_c^{\,2}\left(\omega^2-v_{ab}^{\,2}q_{ab}^{\,2}\right)}}\,q_{ab}\,dq_{ab}\,d\omega \qquad \text{(S17)}$$

It shows that the thermal conductivity is actually an integral of both ω and q_{ab}. Now let's express Eq.

S17 qualitatively by

$$k_{ab}=\int_{\omega} k_{ab,\omega} d\omega \tag{S18}$$

where $k_{ab,\omega}=\int_0^{q_{\max}} f\left(q_{ab},\omega\right) dq_{ab}$, $f\left(q_{ab},\omega\right)$ represents a function of q_{ab} and ω.

The first step of our approach is to consider the total thermal conductivity k_{ab} as a sum of the thermal conductivity per frequency $k_{ab,\omega}$. Figure S2 shows $k_{ab,\omega}$ as function of ω. If we assume a specific ω_1 for example, $k_{ab,\omega 1}$ can be also considered as a sum of thermal conductivity for each q_{ab} at this ω_1. By using $v_{g,ab}=v_{ab}^2 q_{ab}/\omega=\Lambda_{ab}\tau_{ab}^{-1}$, q_{ab} can be expressed as a function of MFP Λ_{ab} and each wave vector is corresponding to a MFP, so $k_{ab,\omega 1}$ is also a sum of thermal conductivity for each Λ_{ab}, , which is the second step of our approach. Here the accumulation function of $k_{ab,\omega 1}$ can be calculated as

$$\alpha_{\omega 1}=\frac{\int_0^{\Lambda_{ab}^*} f\left(\Lambda_{ab},\omega_1\right) d\Lambda_{ab}}{\int_0^{\Lambda_{\max}} f\left(\Lambda_{ab},\omega_1\right) d\Lambda_{ab}} \tag{S19}$$

as shown in Figure S3. Adding all of these accumulation function for $k_{ab,\omega}$, we can get the accumulation function for the total thermal conductivity.

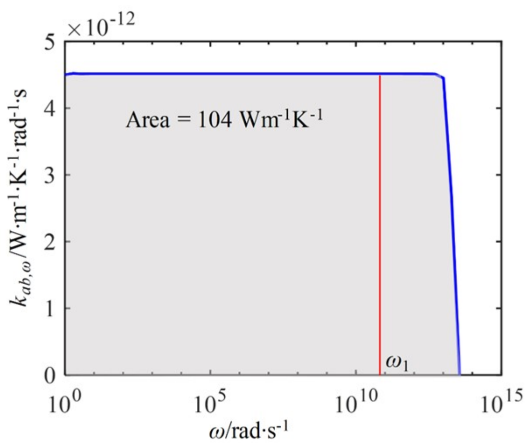

Figure S2. Thermal conductivity per frequency ω as a function of ω, the area formed by this blue line and axis is the in-plane thermal conductivity of MoS_2.

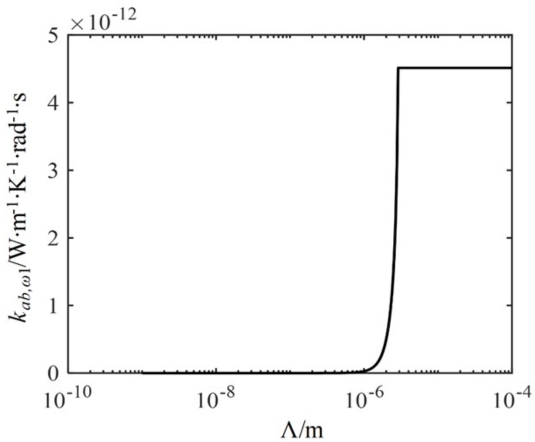

Figure S3. Accumulation function of $k_{ab,\omega 1}$.

In order to better describe this approach, we plot $k_{ab,\ \omega}$ as a function of ω and Λ_{ab} simultaneously as it show in Figure S4a, in which the black volume is formed by a large number of curves. The blue line in Figure S4a is actually the same as that in Figure S2 and the red section at ω_1 is actually the Figure S3 (accumulation function of $k_{ab,\ \omega 1}$). Figure S4c shows the front view of the 3D surface and is also a sum of accumulation function of $k_{ab,\ \omega}$. Therefore, in order to get the accumulation function for total thermal conductivity, we just need to add the accumulation function of $k_{ab,\ \omega}$ for all ω, that is to say, get the projected area of this 3D volume on each section vertical to the Λ_{ab} axis (such as the orange section at Λ_1). The left view of this 3D volume (Figure S4b) shows the maximum projected area (black area) which is the total thermal conductivity and is equal to the area formed by the blue line. Finally, we get the normalized accumulation function for total thermal conductivity as it shown in Figure S4d.

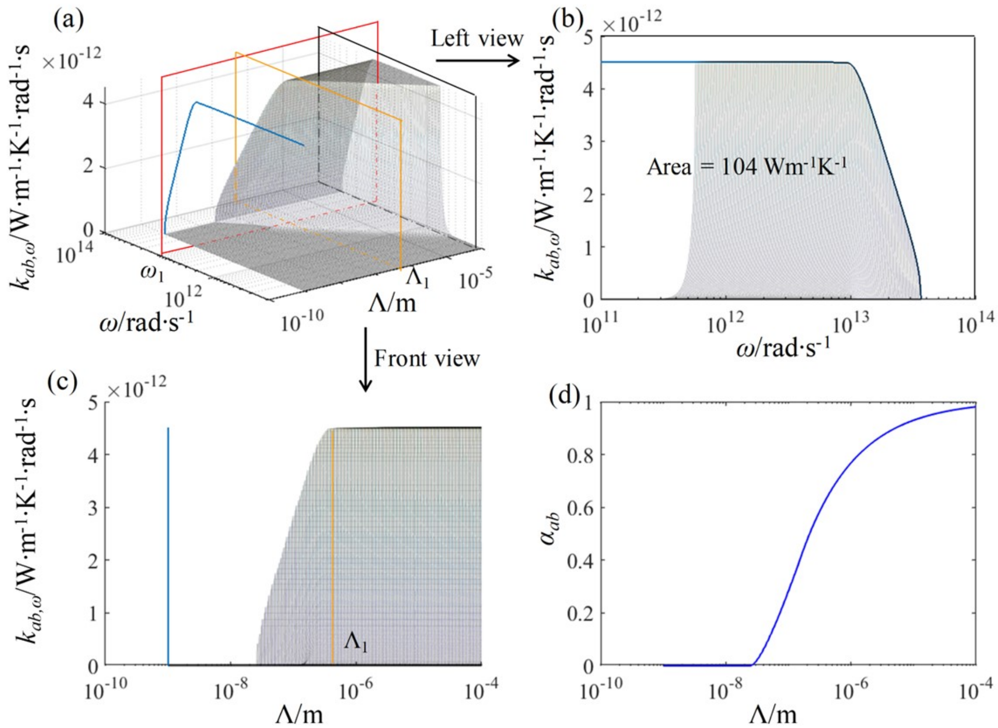

Figure S4. 3D plotting for thermal conductivity per ω as a function of ω and Λ

D. Parameters used in our calculation

Table S1. Parameters used in our calculation, which are extracted from Ref [9] (MoS_2 and graphite), Ref [47] (black P), Ref [48] ($WSe_{2(1-x)}Te_{2x}$), Ref [49] (TiS_2) and Ref [50] ($SnSe_2$). Subscript T, L and Z represent TA, LA and ZA branches, for example, $v_{ab,L}$ means sound velocity of LA branch along the in-plane direction.

Branches	Properties	MoS_2	Graphite	Black P	$WSe_{2(1-x)}Te_{2x}$	TiS_2	$SnSe_2$
TL1	$v_{c,T}$/m·s^{-1}	1938	1487	1090	1572	2825	1499
	$v_{ab,L}$/m·s^{-1}	6850	22152	9450 (ZZ) 4360 (AC)	5003	5284	4144
	$\omega_{c,T}$/10^{12}·rad·s^{-1}	7.77	8.14	3.8	3.4	7.54	4.59
	$\omega_{ab,L}$/10^{12}·rad·s^{-1}	44.5	252	36.8(ZZ) 24.3	26.8	40.8	22.0
	$q_{c,\mathrm{eff}}$/10^{10}·m^{-1}	0.401	0.547	0.349	0.216	0.267	0.306
	$q_{ab,\mathrm{eff}}$/10^{10}·m^{-1}	0.650	1.138	0.389(ZZ) 0.557(AC)	0.536	0.772	0.531

TL2	$v_{c,L}$/m·s^{-1}	3206	4138	4420	2484	4383	2143
	$v_{ab,Z}$/m·s^{-1}	2685	5858	2540(ZZ) 1395(AC)	2442	3008	1499
	$\omega_{c,L}$/10^{12}·rad·s^{-1}	12.8	22.4	14.4	5.5	15.7	6.91
	$\omega_{ab,Z}$/10^{12}·rad·s^{-1}	34.1	94.9	26(ZZ) 12(AC)	20.2	18.8	9.42
	$q_{c,\mathrm{eff}}$/10^{10}·m^{-1}	0.399	0.541	0.326	0.221	0.358	0.332
	$q_{ab,\mathrm{eff}}$/10^{10}·m^{-1}	1.27	1.62	1.02(ZZ) 0.86(AC)	0.827	0.625	0.628
TA	$v_{c,T}$/m·s^{-1}	1938	1487	2540	1572	2825	1499
	$v_{ab,T}$/m·s^{-1}	5372	14236	4190(ZZ) 4190(AC)	3226	3295	1950
	$\omega_{c,T}$/10^{12}·rad·s^{-1}	7.77	8.14	8.8	3.4	7.54	4.59
	$\omega_{ab,T}$/10^{12}·rad·s^{-1}	30.7	162	23.5(ZZ) 14.2(AC)	23.9	31.4	15.7
	$q_{c,\mathrm{eff}}$/10^{10}·m^{-1}	0.401	0.547	0.346	0.216	0.267	0.306
	$q_{ab,\mathrm{eff}}$/10^{10}·m^{-1}	0.571	1.138	0.561(ZZ) 0.339(AC)	0.741	0.953	0.805
	$q_{c,\mathrm{m}}$/10^{10}·m^{-1}	0.401	0.55	0.72	0.258	0.649	0.612
	$q_{ab,\mathrm{m}}$/10^{10}·m^{-1}	1.27	1.62	1.25(ZZ), 0.86(AC)	1.22	1.17	1.05

Sound velocities and cutoff frequencies are used in the calculation by Callaway Model and TDA model, while the sound velocities and cutoff wave vectors are applied in the calculation by BvKS Model. Cutoff wave vectors are obtained by solving equations $\eta_{\mathrm{pub}} = \frac{1}{6\pi^2}\left(q_{c,\mathrm{m}} q_{ab,\mathrm{m}}^2\right)^{1/3}$ and $q_{c,\mathrm{m}} / q_{ab,\mathrm{m}} = \gamma$, where η_{pub} is the number density of primitive unit cells, γ is the anisotropy of cutoff wave vectors in reciprocal space, which is corresponding to the anisotropy of lattice constants.

E. Relaxation times using RTA and first-principle calculations

The relaxation times of the three acoustic phonon branches of MoS_2, calculated by first-principles, are shown in Figure S5.[31] Our RTA model uses just one parameter B to characterize relaxation times due to

Umklapp phonon scattering of all three branches, so a single prediction from our analysis is shown for comparison in Figure S5. The RTA results agree reasonably well with the first principles calculation for frequencies above 1 THz, but deviate from the longer relaxation times exhibited by the ZA phonons in the low frequency region. In the Figure S6, our RTA predictions for graphite are compared with first principles calculations of the relaxation times for graphene.[32] Similar trends are exhibited but the RTA results are shifted to longer relaxation times at all frequencies.

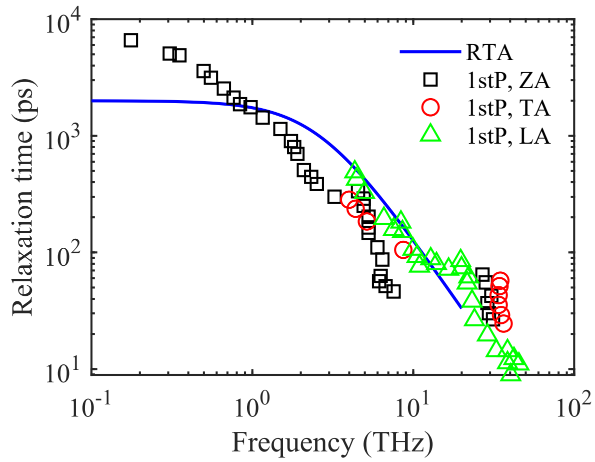

Figure S5. Relaxation times of pure MoS_2 in the in-plane direction at 300K by (a) relaxation time approximation (RTA) and (b) first principle (1stP) calculation by Zhu et al. (Ref [31] in the manuscript).

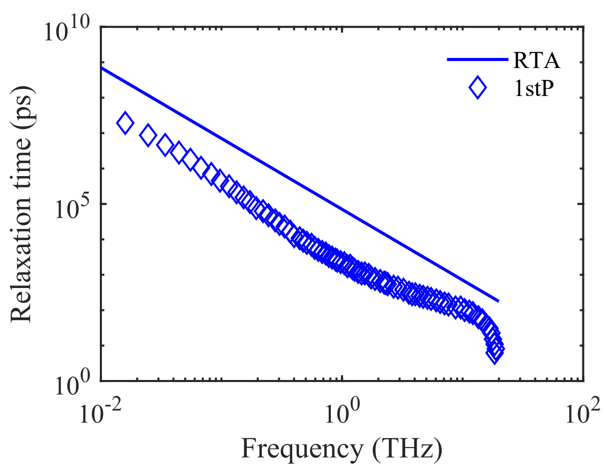

Figure S6. Relaxation times of pure graphite and graphene in the in-plane direction at 300K by (a) relaxation time approximation (RTA) and (b) first principle (1stP) calculation by Taheri et al. (Ref [32] in the manuscript).